ACS ES&T Engineering

pubs.acs.org/estengg

Article

Anchoring NH_2-MIL-101(Fe/Ce) within Melamine Sponge Boosts Rapid Adsorption and Recovery of Phosphate from Water

Junna Yan, Mengyu Ma, Keyi Liu, Yang Bao, and Feihu Li*

Cite This: *ACS EST Engg.* 2023, 3, 467−478

Read Online

ACCESS | Metrics & More | Article Recommendations | Supporting Information

ABSTRACT: Efficient removal and recovery of phosphorus (P) from wastewater is critical for addressing both phosphate rock depletion and eutrophication-related deterioration of surface water quality. Herein, we present a promising platform approach integrating cerium-doped NH_2-MIL-101(Fe) with melamine sponge (MS) scaffolds for rapid and high-efficiency recovery of P from wastewater. The as-prepared MIL-101@sponge composites (denoted as MIL-101@CS, MIL-101@PVDF, and MIL-101@SDBS, respectively) are featured by flexibility and stability according to many characterization techniques. Batch adsorption of P over these composite adsorbents indicates that these MIL-101@sponge composites exhibit a maximum adsorption capacity (e.g., 253.66 mg g^{-1} for MIL-101@CS) at the optimum pH of 6.0 and that adsorption equilibrium can be attained within 150 min and well described by the pseudo-second-order kinetic model. In addition, these composites show a high selectivity for P over carbonate and other common monovalent anions under environmentally relevant conditions. The results of desorption and recycling tests indicate that MIL-101@CS retains good adsorption and desorption efficiency even in a much short operating time (i.e., 5 min), which allows such a composite to be applied in enriching and recovering P efficiently from wastewater via a rapid adsorption/desorption operation. Moreover, the high feasibility of MIL-101@CS in actual scenarios was validated by efficiently enriching the P from a sludge dewatering liquid. Furthermore, the main mechanisms for P adsorption are elucidated from various microstructural characterizations. Overall, this work presents a strategy of integrating MIL-101 with sponge scaffolds for rapidly and efficiently recovering P from wastewater, which may be potentially extended to the recovery of other value-added elements of interest from waste streams.

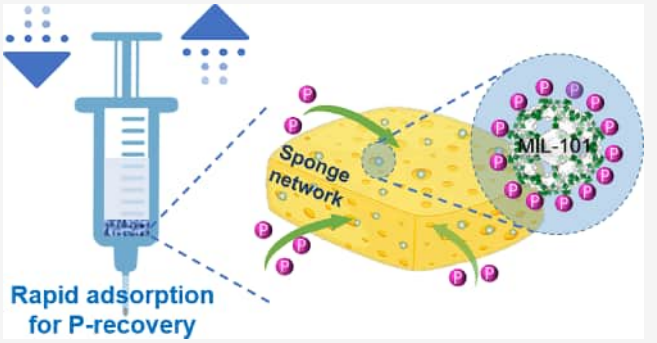

KEYWORDS: *metal−organic frameworks, MIL-101, phosphorus recovery, adsorption kinetics, water purification*

1. INTRODUCTION

Phosphorus (P) is an essential element for the survival of all life on our planet and plays a crucial role in our modern society.[1] Natural P resources, i.e., phosphate rock, are currently being depleted at an extraordinary rate due to an ever-growing demand needed for feeding a global population of over 7.7 billion people. Meanwhile, soil erosion, excessive mining, and unsustainable management of P resources have been aggravating the global P shortage.[2−4] The majority of P lost from the terrestrial environment eventually finds its way into surface waters, leading to water quality concerns (e.g., eutrophication).[5] The current rapid depletion of P resources and the tightening of discharge regulations have encouraged the fast development of a variety of P-recovery techniques from waste streams.[1,5,6] So far, most of these techniques appear to be cost-uncompetitive with phosphate mining; it is therefore of great importance to develop more effective P-recovery techniques.[3,7]

Of various P-recovery techniques invented so far, adsorption occupies a significant role because of its high efficiency, cost-effectiveness, operational simplicity, and environmental friendliness.[7−9] Adsorbents ranging from natural minerals to synthetic materials, from industrial wastes to agricultural straws, and from organic to inorganic materials, etc. have been extensively explored for capturing P from waste streams.[8,10−12] Among the diverse range of adsorbents, metal−organic frameworks (MOFs) offer a very attractive and promising platform for the highly efficient capturing of P from wastewater.[13−20] Water-stable MOFs such as UiO-66, NU-1000, and MIL-101 have been widely used as adsorbents for the removal and recovery of phosphorus. Lin et al.[13] reported that grafting of an amine group to UiO-66 can significantly improve its adsorption capacity and preference

Received: September 29, 2022
Revised: December 29, 2022
Accepted: January 3, 2023
Published: January 12, 2023

https://doi.org/10.1021/acsestengg.2c00324
ACS EST Engg. 2023, 3, 467−478

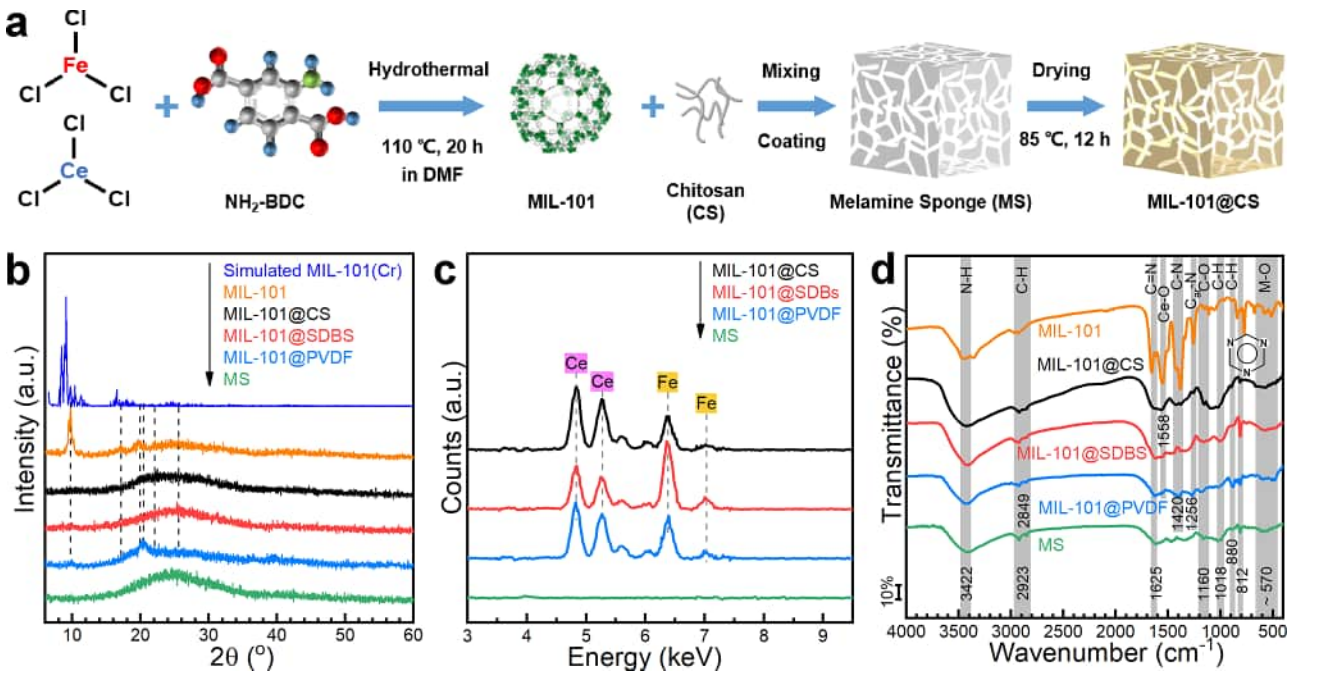

Figure 1. (a) Schematic illustration of the preparation of MIL-101@sponge composites; (b) XRD patterns, (c) XRF spectra, and (d) FT-IR spectra of MS, MIL-101, and MIL-101@sponge composites.

toward P. Xie and coworkers also observed such trends in P adsorption over MIL-101(Fe) and aminated MIL-101(Fe).[14] This improved adsorption affinity by amine groups was further verified in a study assessing the effect of various functional groups on the adsorption performance of UiO-66.[21] Other approaches such as doping by specific P-preferring elements,[16,19,20,22] microstructural tailoring (e.g., creating defect-rich MOFs),[18,23−25] and integrating with various compounds,[17,26−29] have been successfully implemented. However, these nano- and micro-sized MOF adsorbents often suffer from being difficult to fully recover after dispersing in water and are susceptible to lose during the solid−liquid separation process despite their much higher adsorption affinity compared to conventional monolith adsorbents.[30,31]

To overcome the abovementioned obstacles, anchoring or *in situ* growing of nano-sized adsorbents on/inside porous scaffolds such as sponges, aerogels, activated carbon, etc. has shown great promise.[31] Brockgreitens et al.[32] developed a "Crescoating" approach, by which iron nanoparticles have been directly grown on polyurethane sponges that displays a remarkably enhanced adsorption affinity and much more rapid adsorption kinetic for capturing P compared to commercial alternatives. Using a dip-coating method, Ribet and colleagues[33] synthesized a Fe_3O_4-laden Cellulose sponge (referred to as "PEARL"), which can selectively capture up to 99% of P from wastewater at environmentally relevant concentrations. A recent study shows that the melamine sponge (MS) composite anchored with ZIF-8 exhibited excellent oil/water separation performance due to the synergistic effect from the advantages of both ZIF-8 and MS scaffolds.[34] This synergistic effect has also been verified by a most recent study, in which a thiol-laced MOF-based sponge monolith demonstrated high adsorption affinity, fast kinetics, and high selectivity toward Hg(II) ions.[35] Nevertheless, the integration of MOF-based adsorbents with sponge-like porous scaffolds for capturing P from wastewater has not been explored so far. Adsorption behaviors, in particular the kinetics, for P on such MOF@sponge composites are unclear.

Inspired by the above studies and to bridge the gap between the laboratory-scale successes in P recovery using nano-sized MOF adsorbents and the need for simple operations on a pilot-scale, particularly in fully recovering the spent adsorbents, we here present a facile process of anchoring NH_2-MIL-101(Fe/Ce) within MS scaffolds for potential application in P recovery from waste streams. In this study, we use MS as the scaffold due to its desirable properties such as flexibility, large specific surface area, low cost, and high mechanical and chemical stability.[34,36] With the aid of three types of binders, we succeeded in anchoring the as-prepared NH_2-MIL-101(Fe/Ce) particulates inside the MS scaffolds, thereby gaining three MIL-101@sponge composites. We also evaluate the adsorption performance, particularly the rapid adsorption kinetics of these MIL-101@sponge composites toward phosphate from either synthetic water or actual wastewater under environmentally relevant conditions. Using microscopical and spectroscopical techniques, we further characterize the microstructure of these MIL-101@sponge composites and disclose the mechanism of phosphate adsorption. This work presents a promising platform approach integrating MOFs containing P-preferring elements with macroporous MS scaffolds for rapid and high-efficiency P recovery from wastewater. Such a strategy shows promise to be broadly extended to the removal and recovery of other elements of interest from waste streams.

2. MATERIALS AND METHODS

2.1. Chemicals. Iron(III) chloride hexahydrate ($FeCl_3 \cdot 6H_2O$, ≥97.0%), monopotassium phosphate (KH_2PO_4, ≥99.0%), and *N*,*N*-dimethylformamide (DMF, ≥99.5%) were purchased from Sinopharm Chemical Reagent Co., Ltd. (Shanghai, China). Sodium dodecylbenzene sulfonate (SDBS, ≥95%) and cerium chloride heptahydrate ($CeCl_3 \cdot 7H_2O$, 99.9%) were attained from Macklin Biochemical Co., Ltd.

https://doi.org/10.1021/acsestengg.2c00324
ACS EST Engg. 2023, 3, 467−478

(Shanghai, China). Poly(vinylidene fluoride) (PVDF), chitosan (CS), and 2-amino terephthalic acid ($C_8H_7NO_4$, ≥98.0%) were obtained from Aladdin Biochemical Technology Co., Ltd. (Shanghai, China). All chemicals were used as received without further purification. Deionized water was used in preparation solutions.

2.2. Preparation of MIL-101@sponge Composites. Cerium-doped NH_2-MIL-101(Fe) with a Ce/Fe molar ratio of 1.0 was synthesized following the procedure reported elsewhere.[19] The as-prepared brown sample (NH_2-MIL-101(Fe/Ce), denoted as MIL-101) has a Brunauer−Emmett−Teller (BET) surface area of 19 $m^2\ g^{-1}$ as measured at −196 °C using a N_2 gas adsorption analyzer (iQ-AG-MP, Quantachrome, USA). After collecting and washing with deionized water, MIL-101 particles were anchored within MS scaffolds using a facile procedure illustrated in Figure 1a. Briefly, 20 mg of MIL-101 was dispersed ultrasonically in 1 mL of deionized water, followed by mixing and sonicating for 20 min with 2.5 mL of chitosan solution that was prepared by dissolving 200 mg of CS in 0.8% (v/v) acetic acid. A certain volume of the resulting suspension was then pipetted into a clean polypropylene honeycomb-like mold in which each honeycomb had housed an MS cube (10 mm × 10 mm × 10 mm) or cylinder (D 15 mm, H 5.6 mm). The suspension was immediately absorbed by each MS cube/cylinder, which was then dried in an oven at 85 °C for 12 h to achieve anchoring. After cooling to ambient temperature, the MIL-101-anchored MS samples (denoted as MIL-101@CS) were washed several times with methanol, air-dried, and collected for further use.

Next, 30 mg of MIL-101 and 3 mg of CNTs (Nanjing XFNANO Materials Tech Co., Ltd., China) were dispersed ultrasonically in 1 mL of acetone (Sinopharm), followed by mixing and sonicating for 30 min with 2.7 mL of DFM that was pre-dissolved with 220 mg of PVDF. The resulting suspension was then anchored within the MS cubes/cylinders using the same protocol mentioned above for yielding another MIL-101@sponge composite denoted as MIL-101@PVDF.

A certain amount of MS cubes/cylinders were immersed into 20 mL of SDBS (4000 mg L^{-1}) solution with shaking for 30 min. Then the resulting MS samples were washed several times with deionized water and ethanol and dried in an oven at 60 °C for 8 h. Following the above protocol, the SDBS-modified MS samples were subsequently loaded with a given volume of MIL-101 suspension (6 mg of MIL-101 dispersed in 1 mL of deionized water), dried, and washed for attaining the last MIL-101@sponge denoted as MIL-101@SBDS. The ratio of MIL-101 suspension to MS cube/cylinder is 0.6 mL per MS cube/cylinder for all samples.

2.3. Characterization of MIL-101@sponge Composites. X-ray diffraction (XRD) analysis was performed using an XRD-6100 diffractometer (Shimadzu, Japan) with Cu K_α radiation at a tube voltage of 40 kV and a tube current of 30 mA. The step size and scanning rate are 0.02° and 5° min^{-1}, respectively. X-ray fluorescence spectroscopy (XRF) analysis was conducted on a DELTA DC 4000 analyzer (Olympus, USA) with soil mode. A Nicolet iS5 spectrometer (Thermo Fisher, USA) was used for Fourier transform infrared spectroscopy (FT-IR) acquisition with the KBr pellet method. Scanning electron microscopy (SEM) was performed using a SU1510 microscope (Hitachi Japan) at an accelerating voltage of 1.5 kV. X-ray photoelectron spectroscopy (XPS) analysis was conducted on a PHI 5000 spectroscope (Versa Probe, UIVAC-PHI, Japan) equipped with a monochromatized Al K_α X-ray source ($h\nu$ = 1486.6 eV). The binding energy of the C 1s region (284.8 eV) is used for calibrating the binding energy value of other elements.

2.4. Phosphate Adsorption Experiments. A 1000 mg $PO_4^{3-}\ L^{-1}$ of P solution (equivalent to 10.5 mM) was prepared by dissolving the desired amount of monopotassium phosphate in deionized water and used as the stock solution. All adsorption experiments were performed in triplicate at standard atmospheric pressure and ambient temperature (ca. 25 °C). The experiments on the pH effect were carried out in 100 mg $PO_4^{3-}\ L^{-1}$ solutions with a constant adsorbent dosage of 1 g L^{-1} over the pH range of 4 to 10. In brief, 10 mL of P solution with a given pH pre-adjusted with dilute NaOH and HNO_3 was pipetted into a centrifuge tube with a certain amount of MIL-101@sponge composite. The tube was then sealed and mounted on a Labquake tube rotator (Thermo Scientific, USA) for mixing at 60 RPM for 24 h. Next, 5 mL of solution was sampled from the above mixture for pH measurement and P concentration determination. The solution pH value was measured with a pH meter (PHS-25, Rex Electric Chemical). Using a JH723PC visible spectrophotometer (Jinghua Instrument Co. Ltd., China), P concentration was determined following the ascorbic acid method as described previously.[12] The P adsorption capacity can be calculated using the following formula shown as eq. 1:

$$Q = \frac{(C_0 - C_e) \times V}{m} \tag{1}$$

where Q is the adsorption capacity (mg $PO_4^{3-}\ g^{-1}$), m is the mass of the adsorbent (g), C_0 is the initial P concentration (mg $PO_4^{3-}\ L^{-1}$), C_e is the P concentration in solution after 24 h of adsorption by which an equilibrium state was assumed to achieve, and V refers to the total volume of solution (L).

Following the previous recipes for P adsorption over typical inorganic adsorbents,[8,13] the adsorption kinetic study was carried out in 100 mg $PO_4^{3-}\ L^{-1}$ solutions (pH = 6.0 ± 0.1) with a constant adsorbent dosage of 1 g L^{-1} and a contact time over the range of 0 to 20 h. The experimental data are fitted with both the pseudo-first-order and pseudo-second-order models as given in eqs 2 and 3:

$$\ln(Q_e - Q_t) = \ln Q_e - k_1 t \tag{2}$$

$$\frac{t}{Q_t} = \frac{1}{k_2 Q_e^2} + \frac{t}{Q_e} \tag{3}$$

where Q_t is the adsorption capacity (mg $PO_4^{3-}\ g^{-1}$) at a contact time of t (h) and k_1 and k_2 are the pseudo first-order and second-order rate constants, respectively.

Likewise, the adsorption isotherm experiment was conducted with a constant adsorbent dosage of 1 g L^{-1} in P solutions with an increasing initial P concentration varying from 5 to 200 mg L^{-1}. The solution pH and contact time are 6.0 ± 0.1 and 24 h, respectively. Both the Freundlich and the Langmuir models (eqs 4 and 5) are employed to fit the experimental data:

$$Q_e = k_F C_e^{1/n} \tag{4}$$

$$Q_e = \frac{k_L Q_m C_e}{1 + K_L C_e} \tag{5}$$

where k_F (in $(mg^{1-n}\ L^n)\ g^{-1}$) and n are the Friedrich constants, k_L is the Langmuir adsorption energy constant in L mg^{-1}, and

https://doi.org/10.1021/acsestengg.2c00324
ACS EST Engg. 2023, 3, 467−478

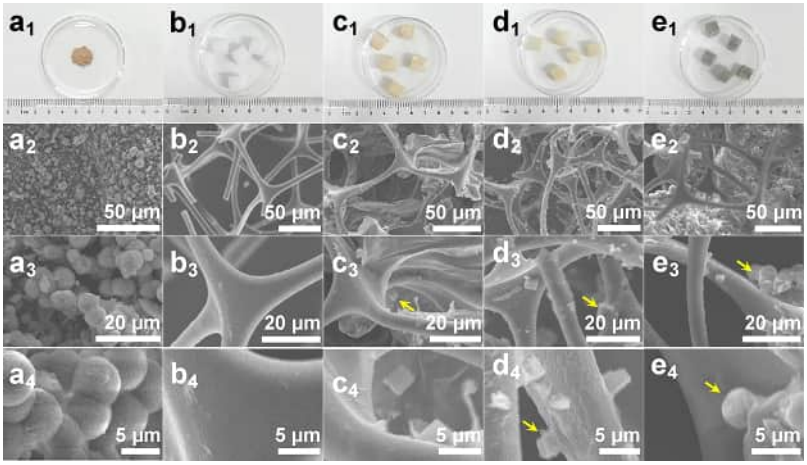

Figure 2. Digital and SEM images of (a) MIL-101, (b) MS, (c) MIL-101@CS, (d) MIL-101@SDBS, and (e) MIL-101@PVDF composites. The anchored MIL-101 particulates are highlighted with yellow arrows.

Q_m is the theoretical maximum adsorption capacity in mg PO_4^{3-} g^{-1}.

2.5. Rapid Adsorption/Desorption Test. Following the same desorption procedure described elsewhere,[11,37] our preliminary experiment has showed that a 0.1 M NaOH solution exhibited the maximum desorption efficiency and thus was employed as the eluent. Both simulated high-P wastewater and actual wastewater (i.e., the sludge dewatering liquid; see Table S1) were used as the effluent being tested. MIL-101@CS was selected for the rapid adsorption/desorption test in a 10 mL syringe (see Figure 5a,b and Movie S1 in the Supporting Information). Briefly, 10 mL of P solution (100 mg L^{-1}) was sucked in and statically adsorbed on a piece of MIL-101@CS cylinder for 5 min before being discharged from the syringe. The spent adsorbent was then regenerated with 5 mL of 0.1 M NaOH solution for 5 min, resulting in a P-enriched eluate and a reclaimed adsorbent, which was then reused consecutively in the abovementioned adsorption/desorption cycle.

3. RESULTS AND DISCUSSION

3.1. Characteristics of MIL-101@sponge Composites. Figure 1b depicts the XRD patterns of pristine MS, MIL-101, and MIL-101@sponge composites. Note that only one broad diffusive reflection centered at $2\theta \approx 24°$ was identified in the MS plot, in agreement with an earlier report unveiling the amorphous nature of MS.[38] The pattern of MIL-101 is featured by a set of well-defined reflections matching the standard XRD pattern of simulated MIL-101(Cr)[39] and those reported elsewhere.[19,40] This finding indicates that the iron and cerium atoms are incorporated into the MIL-101 framework rather than being dispersed in the mixture as oxides or amorphous species. Interestingly, the sharp reflection around $2\theta \approx 10°$ weakened considerably or even disappeared upon anchoring, probably due to a much low dosage of MIL-101 used for anchoring (i.e., ~3.3 mg MIL-101 per each MS cube or cylinder). Likewise, no peaks for CS, PVDF, and SDBS was observed, which is likely due to much low dosage of such agents used in preparing of these composites. The broad diffusive reflection of pristine MS remains upon anchoring of MIL-101, implying the integrality and stability of such composites. In addition, XRF spectra of these MIL-101@sponge composites are inclusive of well-defined principal K-shell emission lines of Fe along with L-shell emission lines of Ce (Figure 1c), implying that MIL-101 particulates were well-anchored inside the MS scaffolds.

FT-IR spectra were also acquired to monitor the evolution of surface functional groups of MS when anchoring MIL-101 (Figure 1d). The characteristic infrared bands observed at 812, 1160, 1256, 1420, 1625, and 3422 cm^{-1} are indicative of triazine ring bending, C−O stretching, aromatic C−N stretching, C−N stretching, C═N stretching, and N−H stretching, respectively.[19,38,41,42] The band at 1558 cm^{-1} is indicative of vibrations of the Ce−O bonds in Ce-MOF that was generated by the reaction of Ce^{3+} with the ligand.[19] The bands at 880 and 1018 cm^{-1} are ascribed to C−H bending, while those at 2849 and 2923 cm^{-1} are assignable to C−H stretching.[41,42] Note that no obvious loss of these bands were observed upon anchoring, indicating that the integration process did not destroy the original structure of the MS scaffolds. Moreover, a weak band at ~570 cm^{-1} ascribable to lattice stretching vibrations of M−O bonds (i.e., Fe−O and Ce−O) was observed in these MIL-101@sponge composites, implying the successful anchoring of MIL-101 inside such a scaffold.

This success was also confirmed by the development of the exterior color and internal microstructure of these MIL-101@sponge composites (Figure 2). The digital images show that the pristine MS cubes turn from white to light brown after anchoring of brown MIL-101 in the case of MIL-101@CS and MIL-101@SDBS (Figure 2a1−d1). Interestingly, MIL-101@PVDF displays a grayish appearance due to the addition of a little number of CNTs along with MIL-101 during the anchoring process (Figure 2e1). Furthermore, SEM images demonstrate that the MS scaffolds are characterized by a three-dimensional (3D) cross-linking network microstructure with a smooth surface as observed previously[34,41,42] and that the near-spherical MIL-101 particulates are evenly anchored on the interior surface of such scaffolds (see the yellow arrows in Figure 2). The low-magnification SEM images (Figure 2c2−e2) show that these MIL-101 particulates are uniformly distributed within such scaffolds. The interior surface of MS becomes rough with various folds and bends upon anchoring of MIL-101, which is likely to increase the specific surface area and thereby the adsorption affinity of such composites. An earlier report on anchoring ZIF-8 on MS has shown that a high

https://doi.org/10.1021/acsestengg.2c00324
ACS EST Engg. 2023, 3, 467−478

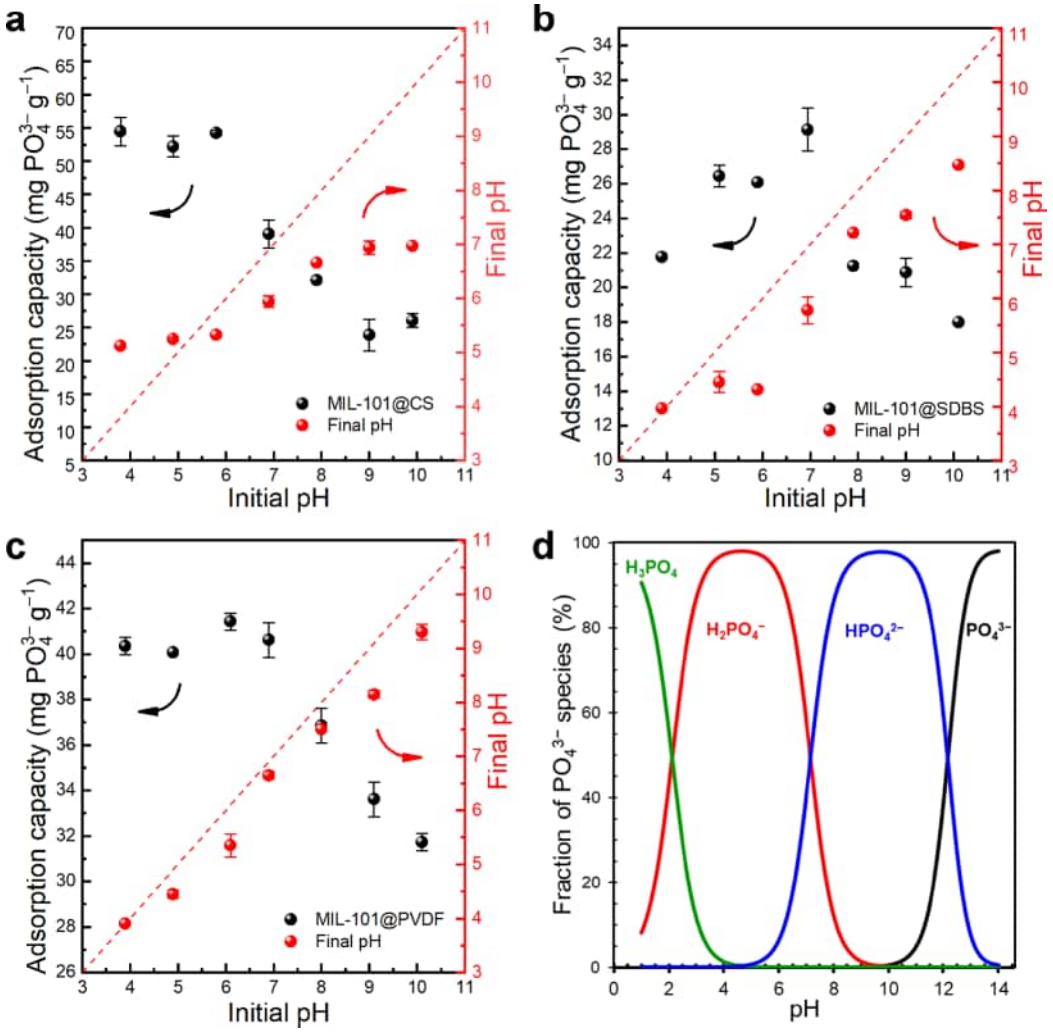

Figure 3. Effects of initial solution pH on P adsorption and the corresponding pH profiles during the adsorption process. (a) MIL-101@CS, (b) MIL-101@SDBS, (c) MIL-101@PVDF, and (d) speciation diagram of 7.35×10^{-4} mol L^{-1} KH_2PO_4 solution at 25 °C (data calculated by using visual MINTEQ 3.1).

dosage of ZIF-8 can be integrated with MS using a surface growth approach,[34] resulting in a much rougher MS surface and a more well-defined XRD pattern of such a composite than the MIL-101@sponge composites in this work. It is therefore reasonable to attribute the above observation of both XRD patterns and SEM images to the lower dose of MIL-101 in the current study. Nevertheless, the porous 3D network of MS retains upon anchoring of MIL-101, confirming the integrity of such composites as observed above by other techniques.

3.2. Effect of pH on Phosphorate Adsorption. The adsorption capacity of MIL-101@sponge composites and the final pH as a function of the initial pH of the adsorption suspension with 100 mg L^{-1} of PO_4^{3-} are shown in Figure 3a–c. The P adsorption capacity of these MIL-101@sponge composites shows a similar trend of increasing initially to reach a maximum followed by gradually dropping down as the pH varies consecutively from 4 to 10. Since dilute nitric acid was used to adjust solution pH in this study, quite a few nitrate ions were introduced, especially in the case of low-pH regions, which is likely to compete with phosphate for the binding sites as discussed later. The introduced nitrate decreases with increasing pH, and thus, the competition decreases accordingly. This may partially explain the increasing trend of P adsorption in the acidic pH region. Moreover, this pH dependence is often observed in P adsorption on MOF-based adsorbents.[30,43−45] Importantly, the final pH values are found to deviate from the initial values (marked with the dashed line) to 0−3 units during the adsorption process, in good agreement with earlier observations.[19,30] This deviation of pH is likely to attribute to the release of protons (H^+) from the ligand exchange between the protonated surface metal hydroxyls (i.e., >Ce/Fe−OH_2^+) of adsorbents and the $H_2PO_4^-$ ions at low pH region and the moderate uptake of free hydroxyl ions from the solution by the surface metal hydroxyls at high pH region.[19]

It is worth noting that the P adsorption capacity maxima of 54.30, 29.13, and 41.69 mg g^{-1} are achieved for MIL-101@CS, MIL-101@SDBS, and MIL-101@PVDF, respectively, when the final pH values of solution fell into the range of 5 to 6, where $H_2PO_4^-$ is the dominant species (Figure 3d). As the final pH increase further to the range of 7 to 8 and beyond, where the dominant P species turns from $H_2PO_4^-$ into HPO_4^{2-} and the surface of MIL-101@sponge composites are likely to be negatively charged,[28,46] the P adsorption capacity of these MIL-101@sponge composites decreases gradually due to the Coulomb repulsion between the negatively charged

https://doi.org/10.1021/acsestengg.2c00324
ACS EST Engg. 2023, 3, 467−478

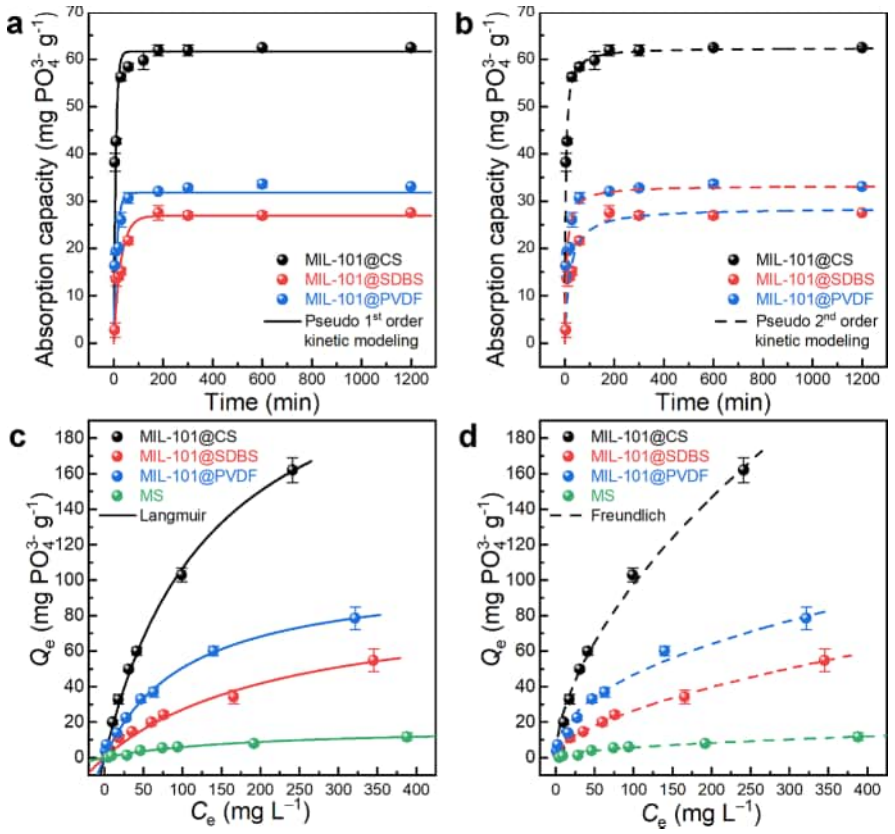

Figure 4. Adsorption kinetics of P onto MIL-101@sponge composites with (a) pseudo-first-order kinetic modeling and (b) pseudo-second-order kinetic modeling (adsorbent dosage = 1 g L^{-1}, P concentration = 100 mg PO_4^{3-} L^{-1}, T = 25 °C); adsorption isotherms of P onto MIL-101@sponge composites with (c) Langmuir model fitting and (d) Freundlich model fitting (adsorbent dosage = 1 g L^{-1}, T = 25 °C, contact time = 24 h).

adsorbent surface and the negative divalent or trivalent P oxyanions. As shown in Figure S1, the point of zero charge (PZC) of the pristine MIL-101 is determined to be 4.1, which also confirms the above speculation of Coulomb repulsion. This observation indicates that P adsorption is most likely involved in both electrostatic attraction and surface complexation under acidic conditions while following a ligand exchange manner at neutral and alkaline pH as reported previously.[19,22,32]

3.3. Effect of Coexisting Species. Since the actual wastewater is complex in composition and usually contains a variety of ions and molecules, such as Cl^-, NO_3^-, SO_4^{2-}, organic matter (OM), etc., which are often likely to compete with phosphate for adsorption sites.[14,17,19,40] To this end, we examined the selectivity of MIL-101@sponge composites for P over other coexisting species including Cl^-, NO_3^-, HCO_3^-, CO_3^{2-}, SO_4^{2-}, and humic acid (HA). The results are given in Figure S2 in the Supporting Information. The P adsorption capacities of all MIL-101@sponge composites show a slight decrease in the presence of carbonate and other monovalent anions (i.e., Cl^-, NO_3^-, and HCO_3^-) with varying concentrations. This finding is most likely due to the formation of outer-sphere surface complexes of these competing ions with a fraction of adsorption sites.[10] This appears to reduce the available adsorption sites for P species via ligand exchange and thereby slightly suppresses P adsorption.[17,19]

Note that SO_4^{2-} ions exhibit a notable competition with phosphate for adsorption sites on these MIL-101@sponge composites (Figure S2). For instance, MIL-101@CS demonstrates a significant decrease in P adsorption capacity from 52.04 to 34.35 mg g^{-1} in the presence of an equivalent mass concentration of SO_4^{2-} (see Figure S2a). The presence of SO_4^{2-}also led to remarkable reductions in P adsorption capacity by 39.12 and 49.32% for MIL-101@SDBS and MIL-101@PVDF, respectively (Figure S2b,c). The competition from sulfate ions is likely attributed to ligand exchange reactions between sulfate ions and the surface hydroxyl groups of the adsorbent and thereby the formation of inner-sphere surface complexes as observed previously.[47,48] Such inner-sphere surface complexes of sulfate appear to be as stable as those of phosphate and therefore negatively impact P adsorption. Apart from inorganic anions, HA ubiquitously dispersing in natural aquatic systems appears to interfere with phosphate adsorption by the preferential occupation of active adsorption sites.[49,50] As expected, the presence of 100 mg L^{-1} of HA resulted in a significant decline of P adsorption capacity by 29.86, 52.82, and 62.35% for MIL-101@CS, MIL-101@SDBS, and MIL-101@PVDF, respectively. It is reasonable to deduce that the surface hydroxyls of MIL-101@sponge (i.e., >Ce/Fe−OH) were strongly bound with HA to form a stable complex that inhibits phosphate adsorption.[51,52]

3.4. Adsorption Kinetics. To investigate the kinetics of P adsorption over these MIL-101@sponge composites, the adsorbate concentration was monitored at varying time intervals from 0 to 20 h. As shown in Figure 4a,b, P adsorption equilibrium was attained within 150 min for all these MIL-101@sponge composites. Adsorption on porous materials generally proceeds in a manner of initially rapid adsorption at the exterior surface of such an adsorbent followed by slow intraparticle diffusion of adsorbate in the adsorbent.[53]

https://doi.org/10.1021/acsestengg.2c00324
ACS EST Engg. 2023, 3, 467−478

Interestingly, the equilibrium time of P adsorption over MIL-101@sponge composites is in good consistence with that of other MIL-101 powder adsorbents for P removal.[17,25,40] This observation is most likely because P adsorption on such MIL-101 adsorbents is governed by the pore diffusion step and that MIL-101 materials often have an approximate mesopore size regardless of their compositions.[54]

To analyze the adsorption behavior of P over such MIL-101@sponge composites, pseudo first- and second-order kinetic models were employed to fit the experimental data. The best-fit kinetic parameters and the fitted results are given in Table S2 and Figure 4a,b, respectively. Compared to the pseudo-first-order model, the pseudo-second-order kinetic model demonstrates higher correlation coefficients (R^2) of 0.976, 0.946, and 0.924 for MIL-101@CS, MIL-101@SDBS, and MIL-101@PVDF, respectively. In addition, the experimental data after adsorption equilibrium ($t \geq 150$ min) are in good agreement with those calculated by the pseudo-second-order model. This result indicates that the P adsorption rate of these MIL-101@sponge composites can be well described and predicted by the pseudo-second-order model and that chemisorption is most likely the rate-limiting step of the adsorption process following the slow intraparticle diffusion step.[40,54] Nevertheless, the relatively rapid adsorption of such MIL-101@sponge composites is believed to be attributed to the abundantly accessible adsorption sites and mesoporous structure of the MIL-101 anchored on the surface of macroporous MS scaffolds.

3.5. Adsorption Isotherms. To illuminate the interaction between P species and adsorbents and estimate the P adsorption capacity of adsorbents, both the Freundlich and Langmuir models are employed to fit the adsorption equilibrium data. The best-fit isotherm parameters and the correlation coefficients (R^2) are given in Table S3, and the fitted plots are depicted in Figure 4dc,. The Langmuir model is based on the assumption of homogeneous adsorbents with identical sites that facilitate monolayer adsorption, while the Freundlich model assumes a heterogeneous system that is not restricted to the formation of the monolayer.[55] Note that all R^2 are ≥0.975 for both models, implying that either the Langmuir model or the Freundlich model can well define the experimental data. Nevertheless, the adsorption isotherms of MIL-101@CS and MIL-101@PVDF fit slightly better with the Langmuir model as indicated by the higher R^2 as compared to the Freundlich model (Table S3), indicating that the P adsorption process is likely to stem from a chemisorption in a monolayer manner.[18] Considering the above observations of the uniform distribution of MIL-101 particles within MS scaffolds, it is rational to speculate the formation of monolayer adsorption between the P species and the active adsorption sites, in particular, of MIL-101@CS and MIL-101@PVDF.[27,54,56] The isotherm of P adsorption over MIL-101@SDBS exhibits a higher correlation coefficient for Freundlich rather than Langmuir, suggesting that P adsorption over such adsorbent appears to occur in a different manner rather than monolayer.[9,18] The maximum P adsorption capacities (Q_m) calculated by using the Langmuir model are 253.66, 90.84, 104.80, and 17.32 mg g^{-1} for MIL-101@CS, MIL-101@SDBS, MIL-101@PVDF, and the pristine MS, respectively. Theoretically, the maximum P adsorption capacity of the pristine MS scaffold is markedly increased by approximately 15 times by anchoring MIL-101 within such a scaffold with the aid of a CS binder, validating the feasibility and merits of this integrating strategy. More importantly, the P adsorption capacities of our MIL-101@sponge composites particularly MIL-101@CS outperform most other MIL-101-based adsorbents reported previously (Table 1), demonstrating the great promise of using such adsorbents for high-efficiency P removal and recovery from waste streams.

Table 1. Comparison of Phosphate Adsorption Capacity of Other MIL-101-Based Adsorbents

adsorbent ID	pH	temperature (°C)	adsorption capacity (mg PO_4^{3-} g^{-1})	ref
MIL-100(Fe)	4	25	93.6	62
MIL-101(Al)	6	25	90.0	25
NH_2-MIL-101(Al)	3–11	45	87.85	40
NH_2-MIL-101(Fe)	2–11	45	94.34	40
MIL-101@Zr(DS)	6.5	25	21.28	49
Fe_2O_3@NH_2-MIL-101(Fe)	7	20	36.6	63
MIL-101(Al)-CS	3–11	45	49.8	64
MIL-101(Fe)-CS	3–11	45	46.8	64
1Ce-MIL-101-NH_2	7	25	341.5	19
MIL-101@CS	6	25	253.66	this study
MIL-101@PVDF	6	25	104.80	this study
MIL-101@SDBS	6	25	90.84	this study

3.6. Rapid Adsorption/Desorption and Recycling Performance. The rapid adsorption/desorption operation was illustrated in Figure 5a. To visualize the adsorption and desorption behaviors of P over MIL-101@CS, a detailed procedure was presented in Figure 5b and Movie S1 using a colored P solution that was prepared by the ascorbic acid method.[57] As evidenced in Figure 5b and Movie S1, MIL-101@CS demonstrates rapid and high-efficiency adsorption and desorption capacity toward P. Figure 5c shows the P adsorption/desorption performance of MIL-101@CS over six consecutive cycles. Note that the removal percentage of P over MIL-101@CS decreases almost linearly with cycle number, from 77.4 to 67.4% in the adsorption efficiency and from 71.0 to 62.8% in the desorption efficiency after six cycles of consecutive adsorption/desorption, respectively. This modest efficiency is likely due to the much short operating time (i.e., 5 min for each adsorption or desorption operation), which is far from that needed for reaching the equilibrium state (e.g., 150 min for attaining an adsorption equilibrium). An attempt to extend the operating time to 10 min led to a significant increase in adsorption efficiency from 77.4 to 92.7% in the first cycle and from 67.4 to 84.0% in the sixth cycle (cf. Figure 5c and Figure S3a). To explore P enrichment performance over MIL-101@CS, the same eluent was reused in every desorption cycle while fresh P solution was used in each adsorption cycle. As shown in Figure S3a, the results reveal that an enrichment factor of 2.05 was achieved in the reclaimed P-enriched eluate (~205 mg L^{-1}) compared to the initial P concentration of the simulated wastewater (i.e., 100 mg L^{-1}) after 10 cycles of enrichment operations. Therefore, it is highly desirable to scale up such a rapid enrichment operation and apply it to real

https://doi.org/10.1021/acsestengg.2c00324
ACS EST Engg. 2023, 3, 467–478

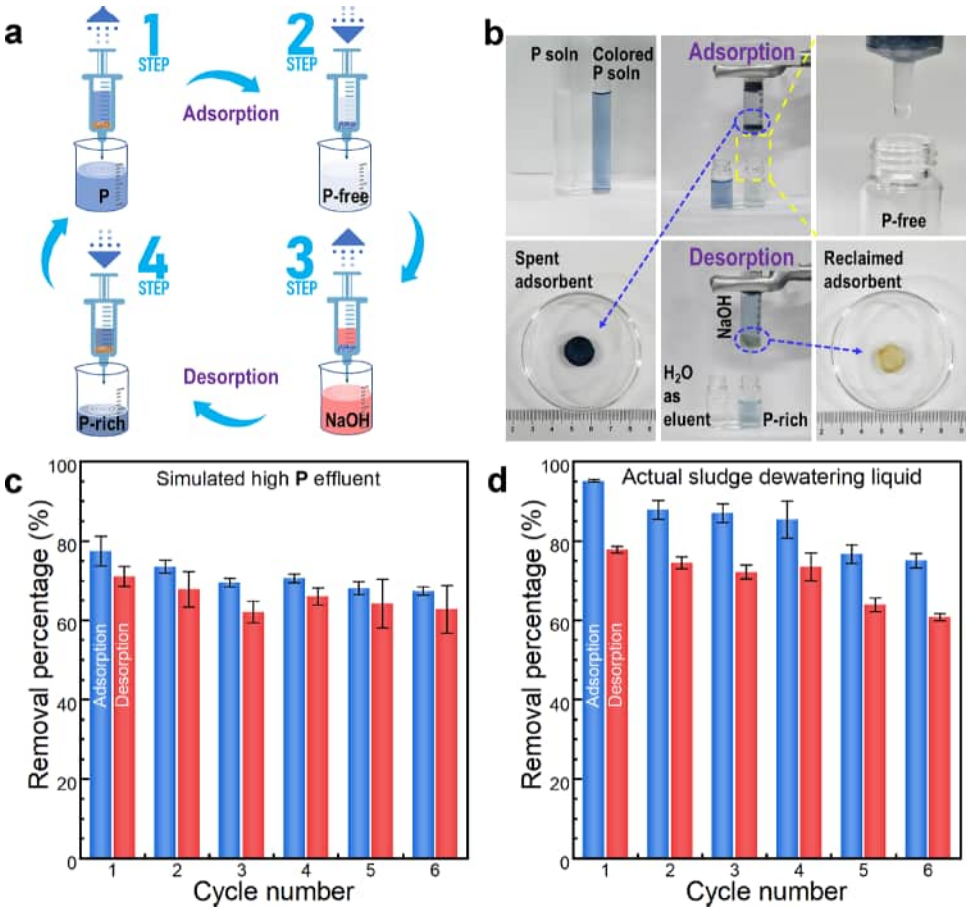

Figure 5. (a) Schematic illustration of the adsorption−desorption operations with a syringe; (b) photos of the adsorption/desorption operations and the spent and reclaimed adsorbents; recycling performance of MIL-101@CS for treating (c) simulated high-P effluent (P = 100 mg L^{-1}), and (d) actual sludge dewatering liquid (P = 13 mg L^{-1}).

wastewater, given its short operating time and ease of operation.

To validate the feasibility of this operation in enriching P from actual wastewater, MIL-101@CS was applied in a sludge dewatering liquid taken from the Nanjing Qiaobei Wastewater Treatment Plant. The characteristic parameters of such a dewatering liquid are given in Table S1. The rapid cycling results depicted in Figure 5d indicate that a similar decreasing trend with the cycle number was observed in both the adsorption and the desorption efficiency and that both efficiencies are higher than those in simulated high-P solution despite the complexity of the actual wastewater composition (Table S1). Note that the actual wastewater contains quite a number of co-occurring calcium (Ca^{2+}) and magnesium ions (Mg^{2+}), both of which can significantly enhance phosphate adsorption as observed previously.[58] This could explain why the recycling performance was higher for the real wastewater over the high P effluent.

In addition, the results of enrichment tests (Figure S3b) show that 1.7 times the amount of P-enriched eluate was obtained after 10 cycles of operations as compared to the initial P level in the actual wastewater (i.e., 13 mg L^{-1}). Furthermore, neither iron nor cerium ions were detectable in the P-enriched eluate according to the inductively coupled plasma optical emission spectroscopic (ICP-OES) data, implying that the anchored MIL-101 particles are fairly resistant to both alkaline leaching and mechanical squeezing without dissolving or shedding. This appears to be ascribed to the strong adhesion of chitosan and the resilience of the macroporous MS scaffolds.[59] The underlying mechanism of P desorption by NaOH is most likely owing to the ion exchange between the adsorbed P species and the free hydroxyl groups.[60] In addition, the digital and SEM images in Figure S4 of MIL-101@CS after six successive adsorption/desorption operations also demonstrate the structural stability of such adsorbents. However, implementing this syringe-based adsorption/desorption on a full scale could be quite challenging at this time. Given the merits of these MOFs@sponge adsorbents, such rapid adsorption/desorption operation may find application in certain point-of-use (POU) scenarios, such as remediation of toxic spills.

3.7. Adsorption Mechanism. To elucidate the underlying mechanisms of P adsorption over MIL-101@sponge, XRD, XRF, FT-IR, and XPS analyses were performed using MIL-101@CS before and after P adsorption as the adsorbent of interest. As shown in Figure 6a, the XRD pattern of MIL-101@CS remains virtually unchanged upon P adsorption, confirming the structural integrity of the adsorbent as observed above. Moreover, a weak peak at 2.01 KeV assignable to the $K_{\alpha 1}$-shell emission line of P was detected in the XRF spectrum (inset in Figure 6b), implying the successful adsorption of P species over MIL-101@CS. FT-IR spectra in Figure 6c also show a new band at 1088 cm^{-1} in the P-sorbed adsorbent, which is attributable to $\nu 3$ vibration (antisymmetric stretching) of

https://doi.org/10.1021/acsestengg.2c00324
ACS EST Engg. 2023, 3, 467−478

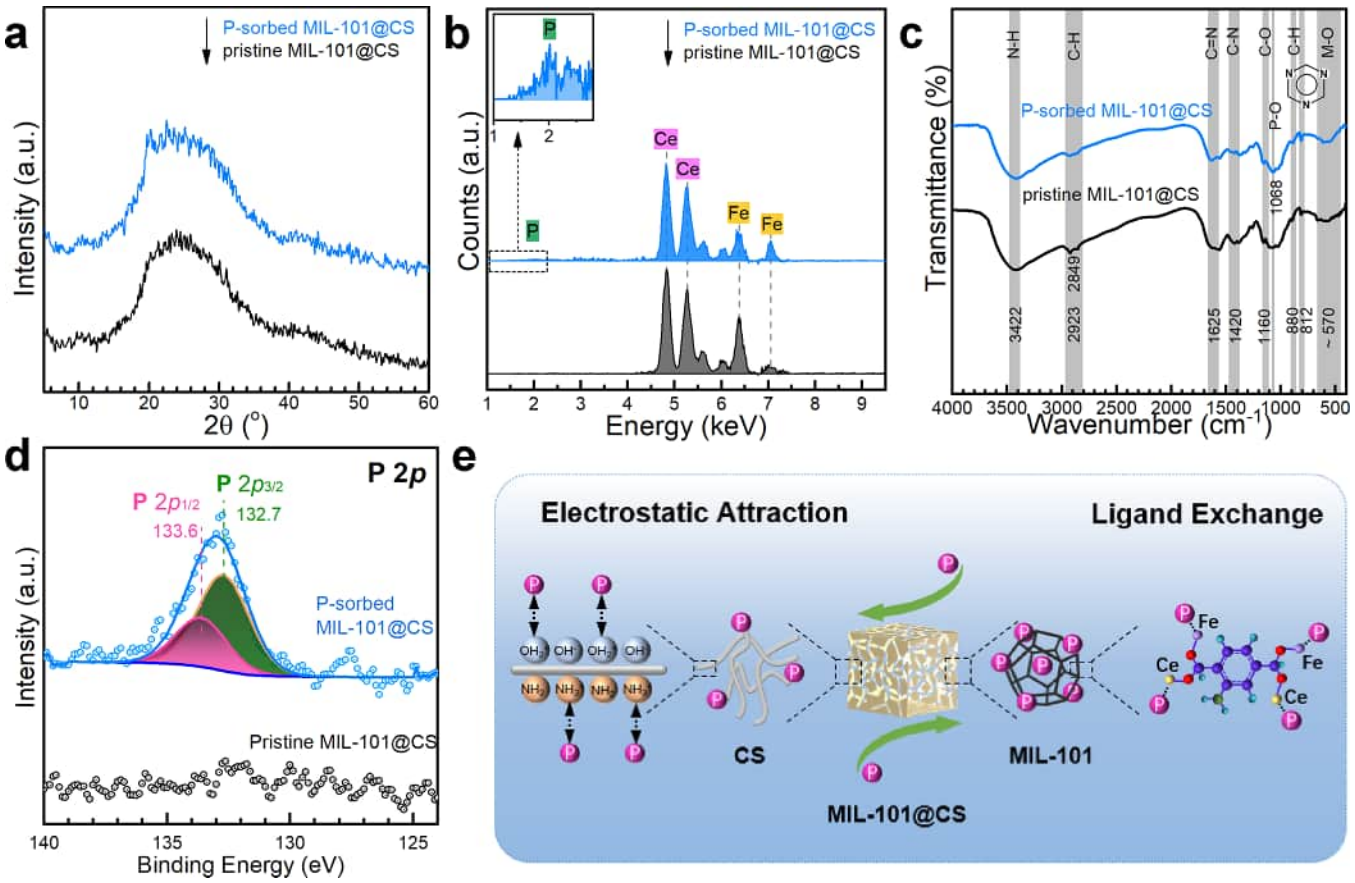

Figure 6. (a) XRD patterns, (b) XRF spectra, (c) FT-IR spectra, and (d) P 2p XPS regions of MIL-101@CS before and after P adsorption; (e) schematic illustration of the proposed P adsorption mechanism.

phosphate.[61] In addition, the band at ~570 cm^{-1}, ascribable to lattice stretching vibrations of M−O bonds, was weakened and shifted slightly toward low-wavenumber regions after P adsorption, suggesting that such groups are involved with P adsorption, most likely via ligand exchange.[19,40,44] The band of amine groups at 3422 cm^{-1} was also slightly weakened upon P adsorption, implying the interaction between P and $-NH_2$ groups.[19,28]

Moreover, XPS spectra have also verified the successful capture of P by MIL-101@CS as indicated by the P 2p peak in the P-sorbed adsorbent (Figure 6d). It is worth noting that the fraction of oxygen in the species of metal oxides and/or phosphate has increased by ~20.5% upon P adsorption as calculated with the data in O 1s XPS regions (Figure S5). Interestingly, the Ce 3d XPS region shifted toward a higher energy direction slightly upon P adsorption (Figure S5), indicating that such an element is chemically involved in P adsorption. Combining the above microstructural evidence with the batch adsorption results, it is reasonable to attribute the primary mechanisms of P adsorption to (i) electrostatic attraction by the positively charged surface of adsorbents (e.g., >Ce/Fe−OH+ 2 and protonated amine groups), particularly at lower pH, and (ii) ligand exchange between phosphate and the surface metal hydroxyls at high-pH regions (Figure 6e).

4. CONCLUSIONS

In summary, NH_2-MIL-101(Fe/Ce) particulates were successfully anchored within macroporous MS scaffolds with the aid of three types of binders, respectively. The as-prepared MIL-101@sponge composites exhibit a high affinity for phosphate with maximum adsorption capacities of 253.66, 104.80, and 90.84 mg g^{-1} at the optimum pH of 6.0 for MIL-101@CS, MIL-101@PVDF, and MIL-101@SDBS, respectively. The adsorption equilibrium can be attained within 150 min and is well-described by the pseudo-second-order kinetic model. Batch adsorption data reveal that carbonate and other common monovalent anions show no competition with phosphate, while sulfate and HA hinder considerably phosphate adsorption over these adsorbents. Additionally, MIL-101@CS exhibits high structural stability and integrity upon leaching with a NaOH eluent and mechanical squeezing. Microstructural analyses of MIL-101@CS before and after adsorption of phosphate reveal that the principal mechanisms are involved in ligand exchange and electrostatic attraction. Benefiting from the large pore structure and flexibility of the MS scaffolds and the high adsorption capacity and rapid kinetics of MIL-101 particulates for phosphate, MIL-101@CS demonstrates the feasibility of high-efficiency enriching and recovering phosphate from phosphorus-containing wastewater (e.g., actual sludge dewatering liquid) via a rapid adsorption/desorption operation in a syringe. Broadly, the strategy of integrating MOFs with macroporous sponge scaffolds for rapid and high-efficiency recovery of phosphate from wastewater can be expanded to the removal and recovery of other elements of interest from waste streams.

https://doi.org/10.1021/acsestengg.2c00324
ACS EST Engg. 2023, 3, 467−478

■ ASSOCIATED CONTENT

Supporting Information

The Supporting Information is available free of charge at https://pubs.acs.org/doi/10.1021/acsestengg.2c00324.

Characteristics of the sludge dewatering liquid; best-fit kinetic and isotherm parameters; ζ potential profile; effect of competing ions; P enrichment performance; morphological characteristics; XPS spectra (PDF)
(Movie S1) Rapid adsorption/desorption operations (MP4)

■ AUTHOR INFORMATION

Corresponding Author

Feihu Li − *Collaborative Innovation Center of Atmospheric Environment and Equipment Technology, Jiangsu Key Laboratory of Atmospheric Environment Monitoring and Pollution Control, School of Environmental Science and Engineering and NUIST Reading Academy, Nanjing University of Information Science and Technology, Nanjing, Jiangsu 210044, China;* orcid.org/0000-0002-2969-8276; Email: fhli@nuist.edu.cn

Authors

Junna Yan − *Collaborative Innovation Center of Atmospheric Environment and Equipment Technology, Jiangsu Key Laboratory of Atmospheric Environment Monitoring and Pollution Control, School of Environmental Science and Engineering, Nanjing University of Information Science and Technology, Nanjing, Jiangsu 210044, China*

Mengyu Ma − *Collaborative Innovation Center of Atmospheric Environment and Equipment Technology, Jiangsu Key Laboratory of Atmospheric Environment Monitoring and Pollution Control, School of Environmental Science and Engineering, Nanjing University of Information Science and Technology, Nanjing, Jiangsu 210044, China*

Keyi Liu − *NUIST Reading Academy, Nanjing University of Information Science and Technology, Nanjing, Jiangsu 210044, China*

Yang Bao − *Collaborative Innovation Center of Atmospheric Environment and Equipment Technology, Jiangsu Key Laboratory of Atmospheric Environment Monitoring and Pollution Control, School of Environmental Science and Engineering, Nanjing University of Information Science and Technology, Nanjing, Jiangsu 210044, China;* orcid.org/0000-0002-5588-2042

Complete contact information is available at: https://pubs.acs.org/10.1021/acsestengg.2c00324

Author Contributions

CRediT: **Junna Yan** data curation, formal analysis, investigation, methodology, validation, visualization, writing-original draft; **Mengyu Ma** investigation, methodology; **Keyi Liu** investigation, methodology; **Yang Bao** investigation, methodology; **Feihu Li** conceptualization, funding acquisition, project administration, supervision, validation, visualization, writing-review & editing.

Notes

The authors declare no competing financial interest.

■ ACKNOWLEDGMENTS

The work was partially supported by the National Natural Science Foundation of China (51002080) and the Innovation Training Programme for Undergraduate Students of NUIST (XJDC202210300251). We would like to thank Dr. Fengying Li for her assistance in the XRF measurement.

■ REFERENCES

(1) Desmidt, E.; Ghyselbrecht, K.; Zhang, Y.; Pinoy, L.; Van der Bruggen, B.; Verstraete, W.; Rabaey, K.; Meesschaert, B. Global Phosphorus Scarcity and Full-Scale P-Recovery Techniques: A Review. *Crit. Rev. Environ. Sci. Technol.* **2015**, *45*, 336−384.

(2) Alewell, C.; Ringeval, B.; Ballabio, C.; Robinson, D. A.; Panagos, P.; Borrelli, P. Global phosphorus shortage will be aggravated by soil erosion. *Nat. Commun.* **2020**, *11*, 4546.

(3) Jupp, A. R.; Beijer, S.; Narain, G. C.; Schipper, W.; Slootweg, J. C. Phosphorus recovery and recycling - closing the loop. *Chem. Soc. Rev.* **2021**, *50*, 87−101.

(4) Vaccari, D. A.; Powers, S. M.; Liu, X. Demand-Driven Model for Global Phosphate Rock Suggests Paths for Phosphorus Sustainability. *Environ. Sci. Technol.* **2019**, *53*, 10417−10425.

(5) Rittmann, B. E.; Mayer, B.; Westerhoff, P.; Edwards, M. Capturing the lost phosphorus. *Chemosphere* **2011**, *84*, 846−853.

(6) Morse, G. K.; Brett, S. W.; Guy, J. A.; Lester, J. N. Review: Phosphorus removal and recovery technologies. *Sci. Total Environ.* **1998**, *212*, 69−81.

(7) Kunhikrishnan, A.; Rahman, M. A.; Lamb, D.; Bolan, N. S.; Saggar, S.; Surapaneni, A.; Chen, C. R. Rare earth elements (REE) for the removal and recovery of phosphorus: A review. *Chemosphere* **2022**, *286*, 131661.

(8) Loganathan, P.; Vigneswaran, S.; Kandasamy, J.; Bolan, N. S. Removal and Recovery of Phosphate From Water Using Sorption. *Crit. Rev. Environ. Sci. Technol.* **2014**, *44*, 847−907.

(9) Wu, B. L.; Wan, J.; Zhang, Y.; Pan, B. C.; Lo, I. M. Selective Phosphate Removal from Water and Wastewater using Sorption: Process Fundamentals and Removal Mechanisms. *Environ. Sci. Technol.* **2020**, *54*, 50−66.

(10) Bacelo, H.; Pintor, A. M. A.; Santos, S. C. R.; Boaventura, R. A. R.; Botelho, C. M. S. Performance and prospects of different adsorbents for phosphorus uptake and recovery from water. *Chem. Eng. J.* **2020**, *381*, 122566.

(11) Li, F.; Jin, J.; Shen, Z.; Ji, H.; Yang, M.; Yin, Y. Removal and recovery of phosphate and fluoride from water with reusable mesoporous Fe_3O_4@mSiO_2@mLDH composites as sorbents. *J. Hazard. Mater.* **2020**, *388*, 121734.

(12) Li, F.; Wu, W.; Li, R.; Fu, X. Adsorption of phosphate by acid-modified fly ash and palygorskite in aqueous solution: Experimental and modeling. *Appl. Clay Sci.* **2016**, *132*, 343−352.

(13) Lin, K. Y. A.; Chen, S. Y.; Jochems, A. P. Zirconium-based metal organic frameworks: Highly selective adsorbents for removal of phosphate from water and urine. *Mater. Chem. Phys.* **2015**, *160*, 168−176.

(14) Xie, Q.; Li, Y.; Lv, Z.; Zhou, H.; Yang, X.; Chen, J.; Guo, H. Effective Adsorption and Removal of Phosphate from Aqueous Solutions and Eutrophic Water by Fe-based MOFs of MIL-101. *Sci. Rep.* **2017**, *7*, 3316.

(15) Dhaka, S.; Kumar, R.; Deep, A.; Kurade, M. B.; Ji, S. W.; Jeon, B. H. Metal-organic frameworks (MOFs) for the removal of emerging contaminants from aquatic environments. *Coord. Chem. Rev.* **2019**, *380*, 330−352.

(16) Min, X.; Wu, X.; Shao, P.; Ren, Z.; Ding, L.; Luo, X. Ultra-high capacity of lanthanum-doped UiO-66 for phosphate capture: Unusual doping of lanthanum by the reduction of coordination number. *Chem. Eng. J.* **2019**, *358*, 321−330.

(17) Zhou, R. Y.; Yu, J. X.; Chi, R. A. Selective removal of phosphate from aqueous solution by MIL-101(Fe)/bagasse composite prepared through bagasse size control. *Environ. Res.* **2020**, *188*, 109817.

(18) Li, M.; Liu, Y.; Li, F.; Shen, C.; Kaneti, Y. V.; Yamauchi, Y.; Yuliarto, B.; Chen, B.; Wang, C. C. Defect-Rich Hierarchical Porous UiO-66(Zr) for Tunable Phosphate Removal. *Environ. Sci. Technol.* **2021**, *55*, 13209−13218.

(19) Liu, M.; Huang, Q.; Li, L.; Zhu, G.; Yang, X.; Wang, S. Cerium-doped MIL-101-NH_2(Fe) as superior adsorbent for simultaneous capture of phosphate and As(V) from Yangzonghai coastal spring water. *J. Hazard. Mater.* **2022**, *423*, 126981.
(20) Zhai, Y.; Li, Y.; Hou, Q.; Zhang, Y.; Zhou, E.; Li, H.; Ai, S. Highly sensitive colorimetric detection and effective adsorption of phosphate based on MOF-808(Zr/Ce). *New J. Chem.* **2022**, *46*, 15405−15413.
(21) Guan, T.; Li, X.; Fang, W.; Wu, D. Efficient removal of phosphate from acidified urine using UiO-66 metal-organic frameworks with varying functional groups. *Appl. Surf. Sci.* **2020**, *501*, 144074.
(22) Liu, M.; Li, S.; Tang, N.; Wang, Y.; Yang, X.; Wang, S. Highly efficient capture of phosphate from water via cerium-doped metal-organic frameworks. *J. Cleaner Prod.* **2020**, *265*, 121782.
(23) Stanton, R.; Trivedi, D. J. Influence of Defects and Linker Exchange on Removal of Phosphate Using MOFs with the Node Structure $M_6(OH)_4(O)_4$ for M = Hf, Zr, or Ce. *Chem. Mater.* **2021**, *33*, 5730−5737.
(24) Wang, L.; Wen, X.; Li, J.; Zeng, P.; Song, Y.; Yu, H. Roles of defects and linker exchange in phosphate adsorption on UiO-66 type metal organic frameworks: Influence of phosphate concentration. *Chem. Eng. J.* **2021**, *405*, 126681.
(25) Li, S.; Lei, T.; Jiang, F.; Liu, M.; Wang, Y.; Wang, S.; Yang, X. Tuning the morphology and adsorption capacity of Al-MIL-101 analogues with Fe^{3+} for phosphorus removal from water. *J. Colloid Interface Sci.* **2020**, *560*, 321−329.
(26) Cheng, Y.; Zhang, J. L. Facile design of UiO-66-NH_2@$La(OH)_3$ composite with enhanced efficiency for phosphate removal. *J. Environ. Chem. Eng.* **2021**, *9*, 104632.
(27) Yang, L.; Zhang, S.; Shan, X.; Ha, C. S.; An, Q.; Xiao, Z.; Wei, L.; Zhai, S. Multifunctional Fe_3O_4/TiO_2/NH_2-UiO-66 with integrated interfacial features for favorable phosphate adsorption. *New J. Chem.* **2022**, *46*, 14091−14102.
(28) Fan, S.; Lu, X.; Li, H.; Du, X.; Huang, X.; Ma, Y.; Wang, J.; Tao, X.; Dang, Z.; Lu, G. Efficient removal of organophosphate esters by ligand functionalized MIL-101 (Fe): Modulated adsorption and DFT calculations. *Chemosphere* **2022**, *302*, 134881.
(29) Wang, J. S.; Yi, X. H.; Xu, X. T.; Ji, H. D.; Alanazi, A. M.; Wang, C. C.; Zhao, C.; Kaneti, Y. V.; Wang, P.; Liu, W.; Yamauchi, Y. Eliminating tetracycline antibiotics matrix via photoactivated sulfate radical-based advanced oxidation process over the immobilized MIL-88A: Batch and continuous experiments. *Chem. Eng. J.* **2022**, *431*, 133213.
(30) Gu, Y.; Xie, D.; Ma, Y.; Qin, W.; Zhang, H.; Wang, G.; Zhang, Y.; Zhao, H. Size Modulation of Zirconium-Based Metal Organic Frameworks for Highly Efficient Phosphate Remediation. *ACS Appl. Mater. Interfaces* **2017**, *9*, 32151−32160.
(31) Luo, J.; Fu, K.; Yu, D.; Hristovski, K.; Westerhoff, P.; Crittenden, J. Review of Advances in Engineering Nanomaterial Adsorbents for Metal Removal and Recovery from Water: Synthesis and Microstructure Impacts. *ACS ES&T Eng.* **2021**, *1*, 623−661.
(32) Brockgreitens, J. W.; Heidari, F.; Abbas, A. Versatile Process for the Preparation of Nanocomposite Sorbents: Phosphorus and Arsenic Removal. *Environ. Sci. Technol.* **2020**, *54*, 9034−9043.
(33) Ribet, S. M.; Shindel, B.; dos Reis, R.; Nandwana, V.; Dravid, V. P. Phosphate Elimination and Recovery Lightweight (PEARL) membrane: A sustainable environmental remediation approach. *PNAS* **2021**, *118*, No. e2102583118.
(34) Lei, Z.; Deng, Y.; Wang, C. Multiphase surface growth of hydrophobic ZIF-8 on melamine sponge for excellent oil/water separation and effective catalysis in a Knoevenagel reaction. *J. Mater. Chem. A* **2018**, *6*, 3258−3263.
(35) Fu, K.; Liu, X.; Lv, C.; Luo, J.; Sun, M.; Luo, S.; Crittenden, J. Superselective Hg(II) Removal from Water Using a Thiol-Laced MOF-Based Sponge Monolith: Performance and Mechanism. *Environ. Sci. Technol.* **2022**, *56*, 2677−2688.
(36) Wang, D.; Song, J.; Lin, S.; Wen, J.; Ma, C.; Yuan, Y.; Lei, M.; Wang, X.; Wang, N.; Wu, H. A Marine-Inspired Hybrid Sponge for Highly Efficient Uranium Extraction from Seawater. *Adv. Funct. Mater.* **2019**, *29*, 1901009.
(37) Bah, A.; Shen, Z.; Yan, J.; Li, F. Coupling the Batch Adsorption Enrichment using Ternary LDHs with Struvite Crystallization in a Fluidized Bed Reactor for High-efficiency Phosphorus Recovery from Wastewater. *ChemRxiv* **2022**, DOI: 10.26434/chemrxiv-2022-wwb35.
(38) Zhang, Y.; Zhang, Q.; Zhang, R. Y.; Liu, S. Z.; Zhou, Y. A superhydrophobic and elastic melamine sponge for oil/water separation. *New J. Chem.* **2019**, *43*, 6343−6349.
(39) Ferey, G.; Mellot-Draznieks, C.; Serre, C.; Millange, F.; Dutour, J.; Surble, S.; Margiolaki, I. A chromium terephthalate-based solid with unusually large pore volumes and surface area. *Science* **2005**, *309*, 2040−2042.
(40) Liu, R.; Chi, L.; Wang, X.; Wang, Y.; Sui, Y.; Xie, T.; Arandiyan, H. Effective and selective adsorption of phosphate from aqueous solution via trivalent-metals-based amino-MIL-101 MOFs. *Chem. Eng. J.* **2019**, *357*, 159−168.
(41) Pham, V. H.; Dickerson, J. H. Superhydrophobic Silanized Melamine Sponges as High Efficiency Oil Absorbent Materials. *ACS Appl. Mater. Interfaces* **2014**, *6*, 14181−14188.
(42) Huang, J.; Xu, Y.; Zhang, X.; Lei, Z.; Chen, C.; Deng, Y.; Wang, C. Polyethylenimine and dithiocarbamate decorated melamine sponges for fast copper (II) ions removal from aqueous solution. *Appl. Surf. Sci.* **2018**, *445*, 471−477.
(43) Wang, J.; Xia, Y. Fe-Substituted Isoreticular Metal-Organic Framework for Efficient and Rapid Removal of Phosphate. *ACS Appl. Nano Mater.* **2019**, *2*, 6492−6502.
(44) Luo, F.; Feng, X.; Li, Y.; Zheng, G.; Zhou, A.; Xie, P.; Wang, Z.; Tao, T.; Long, X.; Wan, J. Magnetic amino-functionalized lanthanum metal-organic framework for selective phosphate removal from water. *Colloids Surf., A* **2021**, *611*, 125906.
(45) Wei, N.; Zheng, X.; Li, Q.; Gong, C.; Ou, H.; Li, Z. Construction of lanthanum modified MOFs graphene oxide composite membrane for high selective phosphorus recovery and water purification. *J. Colloid Interface Sci.* **2020**, *565*, 337−344.
(46) Bao, C.; Zhao, J.; Sun, Y.; Zhao, X.; Zhang, X.; Zhu, Y.; She, X.; Yang, D.; Xing, B. Enhanced degradation of norfloxacin by Ce-mediated Fe-MIL-101: catalytic mechanism, degradation pathways, and potential applications in wastewater treatment. *Environ. Sci.: Nano* **2021**, *8*, 2347−2359.
(47) Ali, M. A.; Dzombak, D. A. Competitive sorption of simple organic acids and sulfate on goethite. *Environ. Sci. Technol.* **1996**, *30*, 1061−1071.
(48) Gu, C.; Wang, Z.; Kubicki, J. D.; Wang, X.; Zhu, M. X-ray Absorption Spectroscopic Quantification and Speciation Modeling of Sulfate Adsorption on Ferrihydrite Surfaces. *Environ. Sci. Technol.* **2016**, *50*, 8067−8076.
(49) Liu, T.; Feng, J.; Wan, Y.; Zheng, S.; Yang, L. ZrO_2 nanoparticles confined in metal organic frameworks for highly effective adsorption of phosphate. *Chemosphere* **2018**, *210*, 907−916.
(50) Thuyavan, Y. L.; Anantharaman, N.; Arthanareeswaran, G.; Ismail, A. F. Adsorptive Removal of Humic Acid by Zirconia Embedded in a Poly(ether sulfone) Membrane. *Ind. Eng. Chem. Res.* **2014**, *53*, 11355−11364.
(51) Koilraj, P.; Sasaki, K. Selective removal of phosphate using La-porous carbon composites from aqueous solutions: Batch and column studies. *Chem. Eng. J.* **2017**, *317*, 1059−1068.
(52) Perassi, I.; Borgnino, L. Adsorption and surface precipitation of phosphate onto $CaCO_3$-montmorillonite: effect of pH, ionic strength and competition with humic acid. *Geoderma* **2014**, *232-234*, 600−608.
(53) Sparks, D. L.Sorption Phenomena on Soils. In *Environmental Soil Chemistry*(Second Edition), Sparks, D. L., Ed. Academic Press: Burlington, 2003; pp. 133−186.
(54) Lee, Y. R.; Yu, K.; Ravi, S.; Ahn, W. S. Selective Adsorption of Rare Earth Elements over Functionalized Cr-MIL-101. *ACS Appl. Mater. Interfaces* **2018**, *10*, 23918−23927.
(55) Dai, J.; Yang, H.; Yan, H.; Shangguan, Y.; Zheng, Q.; Cheng, R. Phosphate adsorption from aqueous solutions by disused adsorbents:

Chitosan hydrogel beads after the removal of copper(II). *Chem. Eng. J.* **2011**, *166*, 970−977.
(56) Mazloomi, S.; Yousefi, M.; Nourmoradi, H.; Shams, M. Evaluation of phosphate removal from aqueous solution using metal organic framework; isotherm, kinetic and thermodynamic study. *J. Environ. Health Sci. Eng.* **2019**, *17*, 209−218.
(57) Clesceri, L. S.; Greenberg, A. E.; Eaton, A. D.*Standard Methods for the Examination of Water and Wastewater*. 20th ed.; American Public Health Association: Washington, DC, 1999; p 4500.
(58) Lin, J.; Zhao, Y.; Zhan, Y.; Wang, Y. Influence of coexisting calcium and magnesium ions on phosphate adsorption onto hydrous iron oxide. *Environ. Sci. Pollut. Res.* **2020**, *27*, 11303−11319.
(59) Wang, M.; Ma, Y.; Sun, Y.; Hong, S.; Lee, S.; Yoon, B.; Chen, L.; Ci, L.; Nam, J.; Chen, X.; Suhr, J. Hierarchical Porous Chitosan Sponges as Robust and Recyclable Adsorbents for Anionic Dye Adsorption. *Sci. Rep.* **2017**, *7*, 18054.
(60) Drenkova-Tuhtan, A.; Schneider, M.; Franzreb, M.; Meyer, C.; Gellermann, C.; Sextl, G.; Mandel, K.; Steinmetz, H. Pilot-scale removal and recovery of dissolved phosphate from secondary wastewater effluents with reusable ZnFeZr adsorbent @ Fe_3O_4/SiO_2 particles with magnetic harvesting. *Water Res.* **2017**, *109*, 77−87.
(61) Stefov, V.; Soptrajanov, B.; Kuzmanovski, I.; Lutz, H. D.; Engelen, B. Infrared and Raman spectra of magnesium ammonium phosphate hexahydrate (struvite) and its isomorphous analogues. III. Spectra of protiated and partially deuterated magnesium ammonium phosphate hexahydrate. *J. Mol. Struct.* **2005**, *752*, 60−67.
(62) Nehra, M.; Dilbaghi, N.; Singhal, N. K.; Hassan, A. A.; Kim, K. H.; Kumar, S. Metal organic frameworks MIL-100(Fe) as an efficient adsorptive material for phosphate management. *Environ. Res.* **2019**, *169*, 229−236.
(63) Li, Y.; Xie, Q.; Hu, Q.; Li, C.; Huang, Z.; Yang, X.; Guo, H. Surface modification of hollow magnetic Fe_3O_4@NH_2-MIL-101(Fe) derived from metal-organic frameworks for enhanced selective removal of phosphates from aqueous solution. *Sci. Rep.* **2016**, *6*, 30651.
(64) Zhang, S.; Ding, J.; Tian, D. Incorporation of MIL-101 (Fe or Al) into chitosan hydrogel adsorbent for phosphate removal: Performance and mechanism. *J. Solid State Chem.* **2022**, *306*, 122709.

https://doi.org/10.1021/acsestengg.2c00324
ACS EST Engg. 2023, 3, 467−478